Supplementary Information

Understanding the domino reaction between 1-diazopropan-2-one and 1,1-dinitroethylene. A molecular electron density theory study of the [3+2] cycloaddition reactions of diazoalkanes with electron-deficient ethylenes

Luis R. Domingo,[a*]Mar Ríos-Gutiérrez[a] and Saeedreza Emamian[b]

[a] Department of Organic Chemistry, University of Valencia, Dr. Moliner 50, E-46100 Burjassot, Valencia, Spain.

[b] Chemistry Department, Shahrood Branch, Islamic Azad University, Shahrood, Iran.

E-mail: domingo@utopia.uv.es

Web: http://www.luisrdomingo.com

Index

1. Theoretical background

1.1 Topological analysis of the Electron Localisation Function (ELF).

Like many other chemical concepts, chemical bonds are defined in a rather ambiguous manner as they are not observable, but rather belong to a representation of the matter at a microscopic level, which is not fully consistent with quantum mechanical principles. To harmonise the chemical description of matter with quantum chemical postulates, several mathematical models have been developed. Among them, the theory of dynamical systems,[1] convincingly introduced by Bader through the theory of atoms in molecules (AIM),[2] has become a powerful method of analysis. The AIM theory enables a partition of the electron density within the molecular space into basins associated with atoms. Another appealing procedure that provides a more straightforward connection between the electron density distribution and the chemical structure is the quantum chemical analysis of the electron localisation function (ELF) of Becke and Edgecombe.[3] ELF constitutes a useful relative measure of the electron pair localisation characterising the corresponding electron density.[4] Within the framework of DFT, ELF is a density-based property that can be interpreted in terms of the positive-definite local Pauli and Thomas Fermi kinetic energy densities in a given system. In the scope of such a framework, these quantities provide key information to evaluate the relative local excess of kinetic energy density associated to the Pauli principle. ELF becomes valued in the range [0,1], the highest values being associated with the spatial positions with higher relative electron localisation.[3-5] After an analysis of the electron density, ELF provides basins of attractors, which are the domains in which the probability of finding an electron pair is maximal. The spatial points in which the gradient of ELF has a maximum value are designated as attractors.[6] ELF basins are classified as core basins, C(...), and valence basins, V(...). The latter are characterised by the synaptic order, *i.e.* the number of atomic valence shells in which they participate. Thus, there are monosynaptic, disynaptic, trisynaptic basins and so on.[7] Monosynaptic basins, labelled V(A), correspond to the lone pairs or non-bonding regions, while disynaptic basins, labelled V(A,B), connect the core of two nuclei A and B and, thus, correspond to a bonding region between A and B. This description recovers the Lewis bonding model, providing a very suggestive graphical representation of the molecular system.

1.2 Bonding evolution theory (BET)

When trying to achieve a better understanding of bonding changes in organic chemical reactions, the so-called BET has proved to be a very useful methodological tool.[8] BET applies Thom's catastrophe theory (CT) concepts[9] to the topological analysis of the gradient field of the ELF.[3]

Within the BET methodology,[10] the structural stability of the critical points of the ELF gradient field is examined for the system of nuclei and electrons 'evolving' along the Born-Oppenheimer energy hypersurface or a given reduced reaction coordinate, *e.g.* the intrinsic reaction coordinate, occurring as a result of the variation in the control space parameters from reactive to product configurations. The chemical process becomes thus rationalised in terms of successive structural stability domains (SSDs), also called phases, comprising structures along the path where the number and type, *e.g.* synaptic orders, of critical points of the gradient field of ELF remain without changes.[10]

Within the BET context, the turning points between these phases are located and the discontinuities or bifurcation catastrophes can be identified. BET allows, thus, characterising unequivocally the behaviour of the dynamical system upon bifurcations associated with the ELF gradient field changing along the reaction coordinate. The different catastrophes in this case correspond to the reduction or the increase of the critical points associated with attractors of electron pairs defining bonding and non-bonding, *e.g.* lone pairs, domains for electron (de)localisation.

A detailed examination of the topology of ELF along the IRC pathway for a given reaction reveals the existence of several catastrophes belonging exclusively to the fold, F and $F^{\dagger}$, and cusp, C and $C^{\dagger}$, elementary types, according to Thom's classification. The F catastrophe merges an attractor and a saddle point into a wandering point, *i.e.* a non-critical point, decreasing the number of basins by 1, whereas $F^{\dagger}$ splits a wandering point into an attractor and a saddle point increasing the number of basins by 1. The † superscript is utilised in those catastrophes where either the number of attractors or the synaptic order increase. The cusp catastrophe C merges two attractors and a saddle point into an attractor decreasing the number of basins by 1, while $C^{\dagger}$ splits an attractor into two attractors and a saddle point increasing the number of basins by 1. The symbol of a catastrophe written in bold is used to mark a catastrophe leading to the formation of the first covalent bond. The analysis of the changes in the number and type of ELF valence basins for the

structures involved along the IRC of the reaction allows establishing a set of points, **Pi**, separating the different phases that characterise the studied molecular mechanism.

Several theoretical studies have shown that the topological analysis of the ELF offers a suitable framework for the study of the changes of electron density.[11] This methodological approach is used as a valuable tool to understand the bonding changes along the reaction path and, consequently, to establish the nature of the electronic rearrangement associated with a given molecular mechanism within a BET perspective.

References

1 R. H. Abraham and C. D. Shaw, Dynamics: The Geometry of Behavior, Addison-Wesley, Redwood City, CA, 1992.

2 R. F. W. Bader, Atoms in Molecules. A Quantum Theory, Claredon Press, Oxford, U.K, 1990.

3 A. D. Becke and K. E. Edgecombe, *J. Chem. Phys.*, 1990, **92**, 5397.

4 (a) B. Silvi, and A. Savin, *Nature*, 1994, **371**, 683; (b) A. Savin, B. Silvi, and F. Colonna, *Can. J. Chem.*, 1996, **74**, 1088.

5 (a) A. Savin, A. D. Becke, J. Flad, R. Nesper, H. Preuss and H. G. Vonschnering, *Angew. Chem. Int. Ed.*, 1991, **30**, 409: (b) A. Savin, R. Nesper, S. Wengert and T. F. Fassler, *Angew. Chem. Int. Ed.*, 1997, **36**, 1809.

6 A. Savin, *J. Chem. Sci.*, 2005, **117**, 473.

7 B. Silvi, *J. Mol. Struct.*, 2002, **614**, 3.

8 X. Krokidis, S. Noury and B.Silvi, *J. Phys. Chem. A*, **1997**, **101**, 7277.

9 (a) R. Thom, *Structural Stability and Morphogenesis: An Outline of a General Theory of Models*, Inc., Reading, Mass (London-Amsterdam, 1976); (b) A. E. R. Woodcock and T. Poston, *A Geometrical Study of Elementary Catastrophes,* (Spinger-Verlag, Berlin, 1974); (c) R. Gilmore, *Catastrophe Theory for Scientists and Engineers* (Dover, New York, 1981).

10 (a) S. Berski, J. Andrés, B. Silvi and L. R. Domingo, *J. Phys. Chem. A*, 2003, **107**, 6014; (b) S. Berski, J. Andrés, B. Silvi and L. R. Domingo, *J. Phys. Chem. A*, 2006, **110**, 13939; (c) V. Polo, J. Andrés, S. Berski, L. R. Domingo and B. Silvi, *J. Phys. Chem. A*, 2008, **112**, 7128; (d) J. Andrés, P. González-Navarrete and V. S. Safont, *Int. J. Quant. Chem.,* 2014, **114**, 1239; (e) J. Andrés, S. Berski, L. R. Domingo, V.

Polo and B. Silvi, *Curr. Org. Chem.*, 2011, **15**, 3566; (f) J. Andrés, L. Gracia, P. González-Navarrete and V. S. Safont, *Comp. Theor. Chem.*, 2015, **1053**, 17.

11 (a) E. Chamorro, P. Fuentealba and A. Savin, *J. Comput. Chem*., 2003, ***24***, 496; (b) E. Chamorro, *J. Chem. Phys.*, 2003, **118**, 8687; (c) E. Chamorro, R. Notario, J. C. Santos and P. Pérez, *Chem. Phys. Lett.*, 2007, **443**, 136; (d) L. R. Domingo, E. Chamorro and P. Pérez, *J. Org. Chem.*, 2008, **73**, 4615; (e) L. R. Domingo, E. Chamorro and P. Pérez, *Org. Biomol. Chem.*, 2010, **8**, 5495; (f) S. Berski and Z. Ciunik, *Mol. Phys.*, 2015, **113**, 765; (g) M. Ríos-Gutiérrez, P. Pérez and L. R. Domingo, *RSC Adv.* **2015**, *5*, 58464.

2. BET study of the 32CA reaction between DAA 10 and DNE 11.

In order to understand the molecular mechanism of the 32CA reaction between DAA **10** and DNE **11**, a BET study of the more favourable C1−C5 reactive channel was performed. BET study shows that this reaction is topologically characterised by ten differentiated phases. Following the notation introduced by Berski *et al.*[1] for representing reaction mechanisms studied within a BET perspective, this 32CA reaction can be associated with the following sequence of catastrophes: $C_3H_4N_2O$ + $C_2H_2N_2O_4$: 9-*CCF*†*F*†*F*†***C***†***C***-0: $C_5H_6N_4O_5$. The populations of the most significant valence basins of the selected points of the IRC are included in Table S1, the ELF attractor positions and basin representations for the points involved in the bond formation processes are shown in Figure S1 and Figure S2, respectively, and the basin-population changes along the reaction path are graphically represented in Figure S3. A representation of the relative energy for the cycloaddition process along the IRC is presented in Figure S4; the relative positions of the points **Pi** defining the phases along the reaction path are shown on the energy curve. A detailed view of the evolution of the ELF in the molecular plane defined by the C1, N3 and C5 atoms is displayed in Figure S5, by using colour-filled maps of the ELF for the points involved in the bond formation processes; in Figure S5, the maps use different colours to represent the ELF value in different regions ranging from blue (no electron localisation) to red (high electron localisation).

Phase I, 3.30 Å ≥ d(C1−C5) > 2.80 Å and 3.22 Å ≥ d(N3−C4) > 3.00 Å, begins at **MC1**, d(C1−C5) = 3.295 Å and d(N3−C4) = 3.217 Å, being a minimum in the PES connecting the separated reagents DAA **10** and DNE **11** with **TS1**. The ELF picture of **MC1** shows the topological characteristics of the separated reagents. Thus, ELF analysis of the DAA framework in **MC1** exhibits a similar bonding pattern to that of DAA **10** (see Table S1 and Figure 1). At the DNE framework, two V(C4,C5) and V'(C4,C5) disynaptic basins, integrating 1.91e and 1.83e, are observed describing the C4=C5 double bond. At **MC1**, there is no GEDT, 0.02e.

Phase II, 2.80 Å ≥ d(C1−C5) > 2.41 Å and 3.00 Å ≥ d(N3−C4) > 2.82 Å, begins at **P1**. This point is established by means of a *C* catastrophe characterised by the merger of the two V(C1) and V'(C1) monosynaptic basins present at **MC1** into a new V(C1) monosynaptic basin integrating 0.51e. This first topological change is mainly the

consequence of the strong decrease of the total electron density gathered at the C1 carbon by 0.48e from **MC1**. At **P1**, a slight amount of GEDT is observed, 0.08e.

Phase III, 2.41 Å ≥ d(C1–C5) > 2.08 Å and 2.82 Å ≥ d(N3–C4) > 2.68 Å, begins at **P2**, which is also associated with a *C* catastrophe. At this point, the two V(C4,C5) and V'(C4,C5) disynaptic basins associated with the C4–C5 double bond merge into a new V(C4,C5) disynaptic basin with a population of 3.78e. Consequently, *phase III* is related to the breaking of the C4=C5 double bond of DNE **11**. At **P2**, the GEDT has increased by 0.10e.

Phase IV, 2.08 Å ≥ d(C1–C5) > 2.06 Å and 2.68 Å ≥ d(N3–C4) > 2.67 Å, which begins at **P3**, is a extremely short phase determined by a $F^{\dagger}$ catastrophe (see Figure S4). This catastrophe implies the creation of a new V(C5) monosynaptic basin at the C5 carbon, which corresponds to the most electrophilic center of DNE **11**, with an initial population of 0.14e. The population of this monosynaptic basin mainly proceeds from the depopulation of the V(C4,C5) disynaptic basin to 3.69e. On the other hand, the V(C1) monosynaptic basin has reached a population of 0.90e. Note that the two V(C1) and V(C5) monosynaptic basins are required for the formation of the C1–C5 single bond in *phase VII*.[2] At **P3**, the GEDT has strongly increased to 0.32e.

At *phase V*, 2.06 Å ≥ d(C1–C5) > 2.04 Å and 2.67 Å ≥ d(N3–C4) > 2.66 Å, which is also a very short phase beginning at **P4**, the most notable topological change is the appearance of a V(N2) monosynaptic basin, integrating 1.20e, by means of a $F^{\dagger}$ catastrophe. The electron density of this new V(N2) monosynaptic basin, which is associated with the N2 lone pair present at pyrazoline **15**, comes mainly from the strong depopulation of the V(C1,C2) monosynaptic basin from 3.42e at **P3** to 2.27e at **P4**, *i.e.* 1.15e. The GEDT has slightly increased by 0.02e.

Phase VI, 2.04 Å ≥ d(C1–C5) > 2.01 Å and 2.66 Å ≥ d(N3–C4) > 2.64 Å, begins at **P5**. This point is defined by a $F^{\dagger}$ catastrophe consisting of the creation of a new V(C4) monosynaptic basin at the C4 carbon with an initial population of 0.52e (see **P5** in Figure S1 and Figure S2). This electron density coincides exactly with the electron density lost by the V(C4,C5) disynaptic basin to 3.14e. On the other hand, the V(C1) and V(C5) monosynaptic basins have reached populations of 0.93e and 0.17e. In this phase, the TS of the reaction, **TS1**, d(C1–C5) = 2.025 Å and d(N3–C4) = 2.653 Å, is found. At this structure, only slight changes in the electron density distribution with

respect to that found at **P5** are observed. At **P5**, the GEDT scarcely varies; the value of 0.35e at **TS1** indicates this *zw-type* 32CA has a high polar nature.

At the long *phase VII*, 2.01 Å ≥ d(C1–C5) > 1.65 Å and 2.64 Å ≥ d(N3–C4) > 2.37 Å, which begins at **P6**, the first most relevant topological change along the reaction path takes place: the two V(C1) and V(C5) monosynaptic basins present in the previous phase merge into a new V(C1,C5) disynaptic basin presenting an initial population of 1.17e (see **P6** in Figure S1 and Figure S2 and the merger of V(C1) and V(C5), in green in **P5**, into the new V(C1,C5), in blue in **P6**, in Figure S3). This significant topological change, which is associated with a *C* catastrophe, indicates that the formation of the first C1–C5 single bond has already begun at a distance of *ca.* 2.01 Å by a C-to-C coupling of the two C1 and C5 *pseudoradical* centers.[3] In addition, the higher ELF basin population of the V(C1) monosynaptic basin than that of the V(C5) one reveals that the former has a considerably larger contribution in the C1–C5 bond formation than the latter (see **P6** in Figure S5). At **P6**, the maximum GEDT along the 32CA reaction is observed with the formation of the first single bond, 0.38e.

Phase VIII, 1.65 Å ≥ d(C1–C5) > 1.58 Å and 2.37 Å ≥ d(N3–C4) > 1.82 Å, begins at **P7**. This point is characterised by a *C* catastrophe associated with the merger of the two V(N2,N3) and V'(N2,N3) disynaptic basins, integrating 1.58e and 1.73e at **P6**, into a new V(N2,N3) disynaptic basin integrating 2.98e, as a consequence of the loss of a total population of 0.33e in the N2–N3 bonding region. This lost electron density is mainly gathered at the V(N2) monosynaptic basin, which has strongly increased its population to 2.15e. The GEDT maintains the same value as in the previous phase.

Phase IX, 1.58 Å ≥ d(C1–C5) > 1.57 Å and 1.82 Å ≥ d(N3–C4) > 1.69 Å, begins at **P8**. At this point, a singular topological change occurs: the V(N3) monosynaptic basin associated with the N3 lone pair present at 1-pyrazoline **15** splits into two new V(N3) and V'(N3) monosynaptic basins, integrating 3.07e and 0.49e, by means of a $C^{\dagger}$ catastrophe (see **P8** in Figure S1 and Figure S2). On the other hand, the V(C4) monosynaptic basin has increased its population until reaching 0.96e. Note that the two V'(N3) and V(C4) monosynaptic basins are demanded for the formation of the N3–C4 single bond in the next phase. At **P8**, the GEDT has strongly decreased to 0.14e as a consequence of a retro-donation process taking place along the formation of the second N3–C4 single bond.

The last *phase X*, 1.57 Å ≥ d(C1–C5) ≥ 1.53 Å and 1.69 Å ≥ d(N3–C4) ≥ 1.50 Å, begins at **P9**, characterised by a *C* catastrophe, and ends at 1-pyrazoline **15**, d(C1–C5) = 1.534 Å and d(N3–C4) = 1.503 Å. The second most relevant topological change along the reaction path takes place at **P9**: the two V'(N3) and V(C4) monosynaptic basins present in the previous phase merge into a new V(N3,C4) disynaptic basins presenting an initial population of 1.62e (see **P9** in Figure S1 and Figure S2, and the merger of V(N3) and V(C4), in red and green in **P8**, into the new V(N3,C4), in blue in **P9**, in Figure S3). This notable topological change indicates that the formation of the second N3–C4 single bond has already started at a distance of *ca.* 1.69 Å by the sharing the electron density of two N3 and C4 *pseudoradical* centers. Note that the different shape of the V'(N3) monosynaptic basin shown in Figure S2 and the orange colour at the V'(N3) region in Figure S5 allows relating this V'(N3) monosynaptic basin with a N3 *pseudoradical* center. This model for the formation of heteroatom-carbon single bonds is similar to that found for the C–O single bond formation in the second stage of the cycloaddition reactions of carbenoid intermediates with CO_2.[4] The GEDT has decreased until reaching an almost null value, 0.06e.

Finally, at pyrazoline **15**, only changes in the ELF basin populations with respect to **P9** are observed. The C1–N2 and N2–N3 bonding regions of the DAA framework are described by one V(C1,N2) disynaptic basin integrating 1.80e and one V(N2,N3) disynaptic basin with a population of 2.51e, emphasising the single bond nature of both regions. The low population of the V(C1,N2) disynaptic basin, together with the high population of the V(N2) and V(N3) monosynaptic basins, 2.71e and 2.83e, denotes the slight polarisation of the C1–N2 and N3–C4 single bonds, the population of the V(N3,C4) disynaptic basin being 1.86e. On the other hand, the C4–C5 bonding region of the DNE moiety is characterised by one V(C4,C5) disynaptic basin integrating 2.04e, while the first formed C1–C5 single bond acquires a population of 1.91e.

Some appealing conclusions can be drawn from this BET study: i) ten differentiated phases associated with the creation or disappearance of valence basins are distinguished along the C1–C5 regioisomeric reaction channel; ii) formation of the C1–C5 single bond follows the recently proposed pattern:[2] a) depopulation of the C1–N2 and C4–C5 bonding regions, b) formation of two non-bonding V(C1) and V(C5) monosynaptic basins and c) formation of a new V(C4,C5) disynaptic basin through the merger of the electron density of the aforementioned monosynaptic basins. Formation

of the C1−C5 single bond begins at *Phase VII* at a distance of 2.01 Å; iii) the presence of the two strong electron-withdrawing nitro groups in DNE **11** makes that the V(C5) monosynaptic basin involved in the formation of the C1−C5 single bond presents a low population, 0.17e; iv) a different behaviour is found for the formation of the N3−C4 single bond. Formation of the N3−C4 single bond begins with the creation of a new V(N3,C4) disynaptic basin at the last *phase X* at the very short distance of 1.69Å. The electron population of this new disynaptic basin proceeds from the electron density of one V(C4) monosynaptic basin created at the α position of the two nitro groups, and one V'(N3) monosynaptic basin associated with the N3 nitrogen lone pairs of DAA **10**. At this phase, the V(C1,C5) disynaptic basin has reached a 97% of its population in pyrazoline **15**; v) this behaviour indicates that this *zw-type* 32CA reaction takes place through a *two-stage one-step* mechanism;[5] and vi) formation of the first C1−C5 single bond begins by a two-center interaction involving the most nucleophilic center of DAA **10**, the C1 carbon, and the most electrophilic center of DNE **11**, the C4 carbon, a behaviour anticipated by the analysis of the electrophilic and nucleophilic Parr functions.

References

1. S. Berski, J. Andrés, B. Silvi and L. R. Domingo, *J. Phys. Chem. A*, 2006, **110**, 13939.
2. L. R. Domingo, *RSC Adv.*, 2014, **4**, 32415.
3. L. R. Domingo, E. Chamorro and P. Pérez, *Lett. Org. Chem.*, 2010, **7**, 432.
4. L. R. Domingo, M. Ríos-Gutiérrez, E. Chamorro and P. Pérez, *Theor. Chem. Acc.*, 2017, **136**, 1.
5. L. R. Domingo, J. A. Saéz, R. J. Zaragozá and M. Arnó, *J. Org. Chem*., 2008, **73**, 8791.

Table S1. Valence basin populations N calculated from the ELF of the IRC points, **P1**–**P9**, defining the ten phases characterising the molecular mechanism of the most favourable reactive channel associated with the 32CA reaction between DAA **10** and DNE **11**. The stationary points **MC1** and 1-pyrazoline **15** are also included. Distances are given in Å, while the GEDT obtained by NBO analysis is given in e.

Phases	*I*	*II*	*III*	*IV*	*V*	*VI*	*VII*	*VIII*	*IX*	*X*
Catastrophes		*C*	*C*	*F†*	*F†*	*F†*	***C***	*C*	*C†*	***C***	
	MC1	**P1**	**P2**	**P3**	**P4**	**P5**	**P6**	**P7**	**P8**	**P9**	**15**
d(C1–C5)	3.295	2.803	2.407	2.076	2.057	2.044	2.006	1.654	1.576	1.567	1.534
d(N3–C4)	3.217	3.001	2.815	2.675	2.667	2.661	2.644	2.371	1.816	1.689	1.503
GEDT	0.02	0.08	0.18	0.32	0.34	0.35	0.38	0.38	0.14	0.06	–0.04
V(C1,N2)	3.07	3.12	3.18	3.42	2.27	2.23	2.15	1.77	1.81	1.83	1.80
V(N2)					1.20	1.24	1.36	2.15	2.54	2.61	2.71
V(N2,N3)	1.79	1.77	1.78	1.64	1.62	1.61	1.58	2.98	2.67	2.64	2.51
V’(N2,N3)	1.88	1.87	1.80	1.75	1.73	1.73	1.73				
V(C4,C5)	1.91	2.00	3.78	3.69	3.66	3.14	3.09	2.54	2.13	2.10	2.04
V’(C4,C5)	1.83	1.76									
V(C1)	0.43	0.51	0.68	0.90	0.92	0.93					
V’(C1)	0.55										
V(C5)				0.14	0.16	0.17					
V(C1,C5)							1.17	1.71	1.83	1.85	1.91
V(N3)	3.76	3.73	3.69	3.56	3.55	3.55	3.54	3.48	3.07	2.96	2.83
V’(N3)									0.49		
V(C4)						0.52	0.55	0.78	0.96		
V(N3,C4)										1.62	1.86

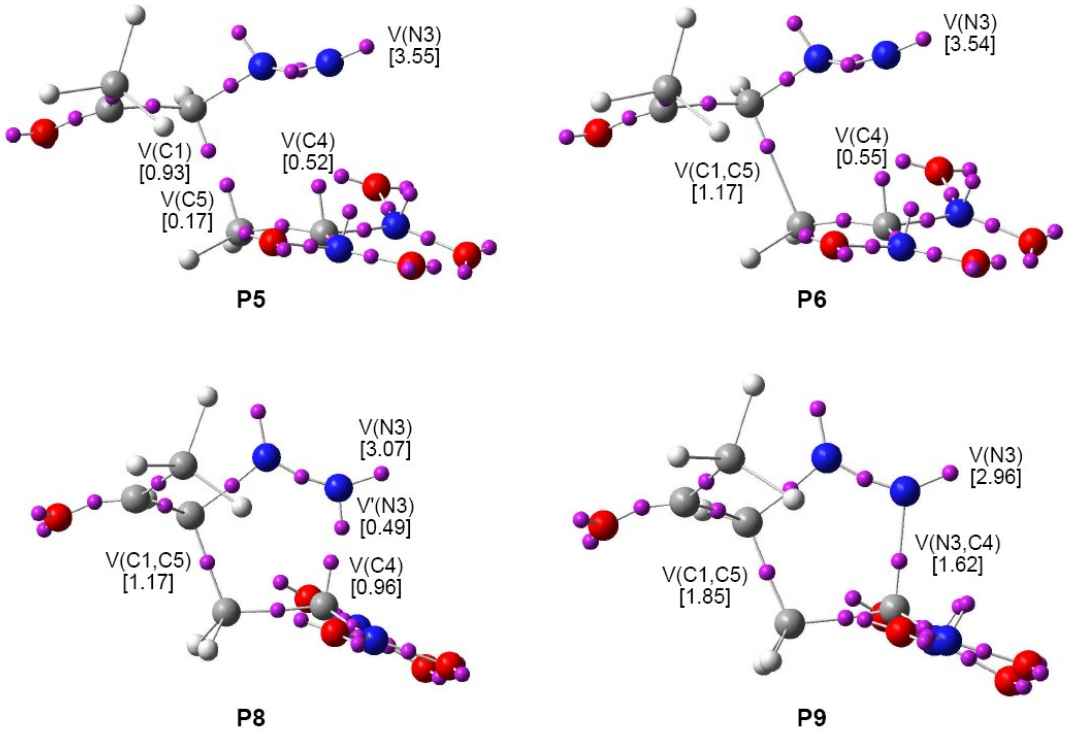

Figure S1. ELF attractor positions for the most relevant points along the IRC involved in the formation of the C1–C5 and N3–C4 single bonds along the most favourable reactive channel associated with the 32CA reaction of DAA **10** with DNE **11**. The electron-populations, in e, are given in brackets.

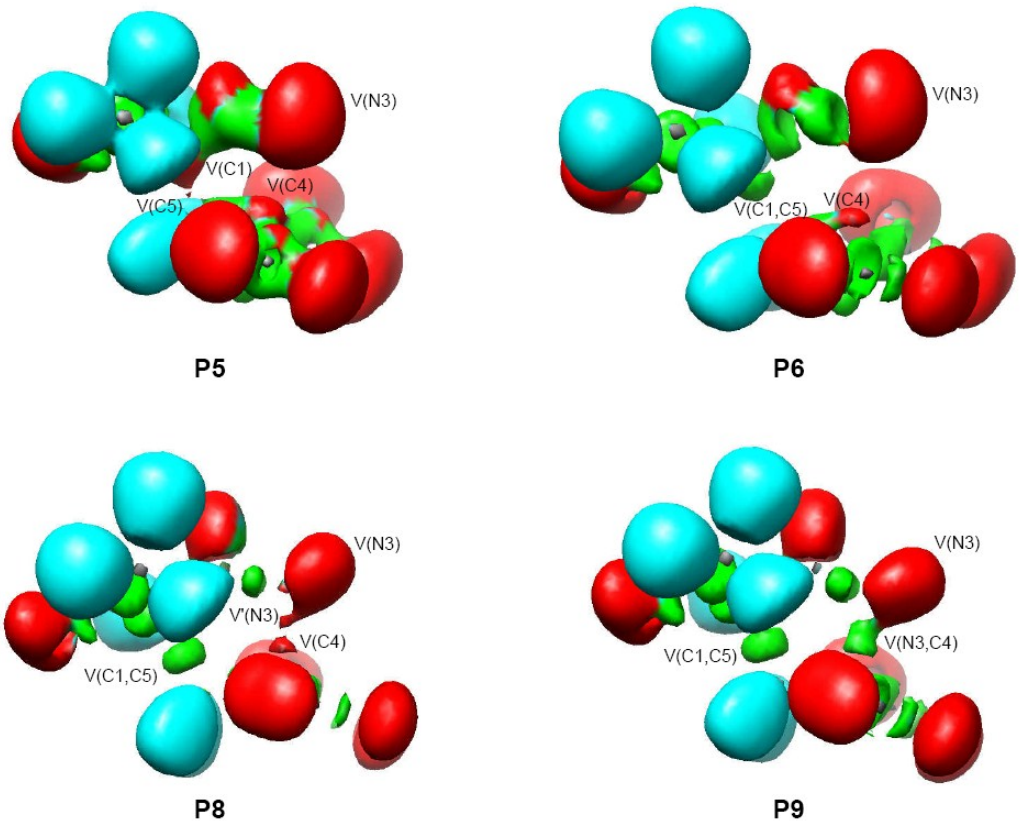

Figure S2. ELF valence basin representations for the points involved in the bond formation processes along the IRC path of the 32CA reaction between DAA **10** with DNE **11**.

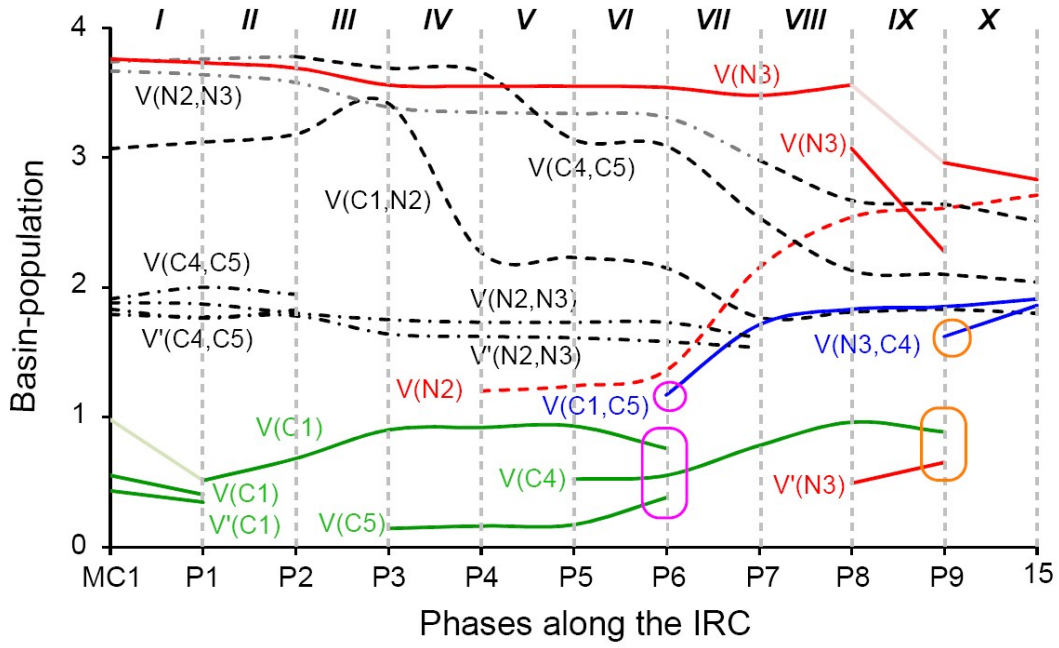

Figure S3. Graphical representation of the basin population changes along the 32CA reaction between DAA **10** with DNE **11**. Dash dotted curves represent bonding regions described by two basins, dashed curves represent bonding regions described by only one basin and lined curves represent the basins directly involved in the formation of the new single bonds; black curves represent basins that do not participate in the bond formation processes, grey curves represent the sum of basins characterising a bonding region, the red colour is for lone pairs, green for *pseudoradical* centers and blue for the new formed single bonds.

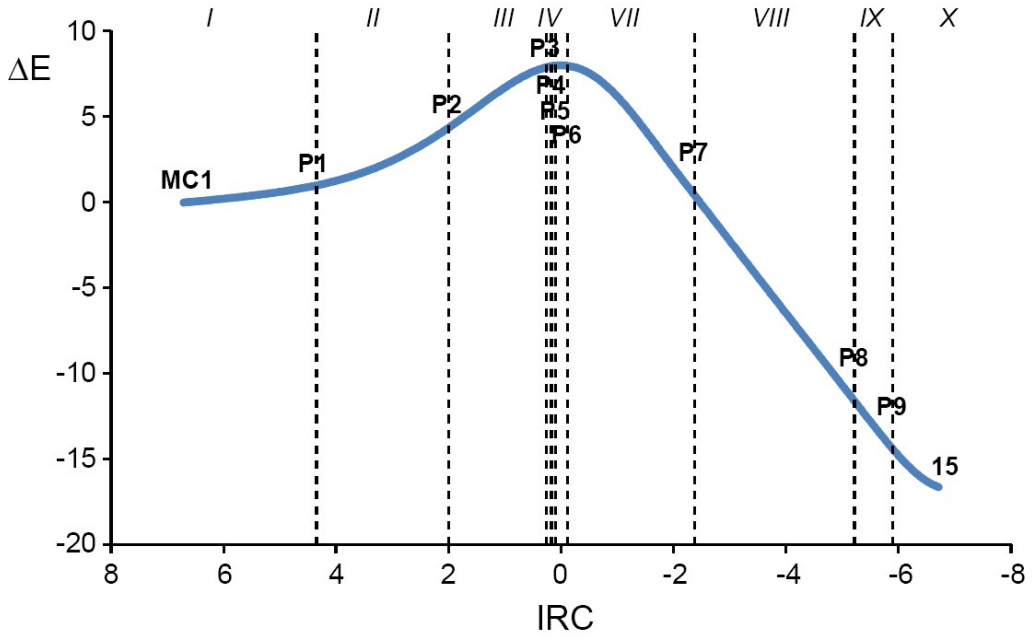

Figure S4. Relative energy (ΔE, in kcal·mol^{-1}) variations along the IRC (amu$^{1/2}$Bohr) associated with the 32CA reaction between DAA **10** with DNE **11** showing the relative positions of the selected points separating the ten topological phases along the reaction path.

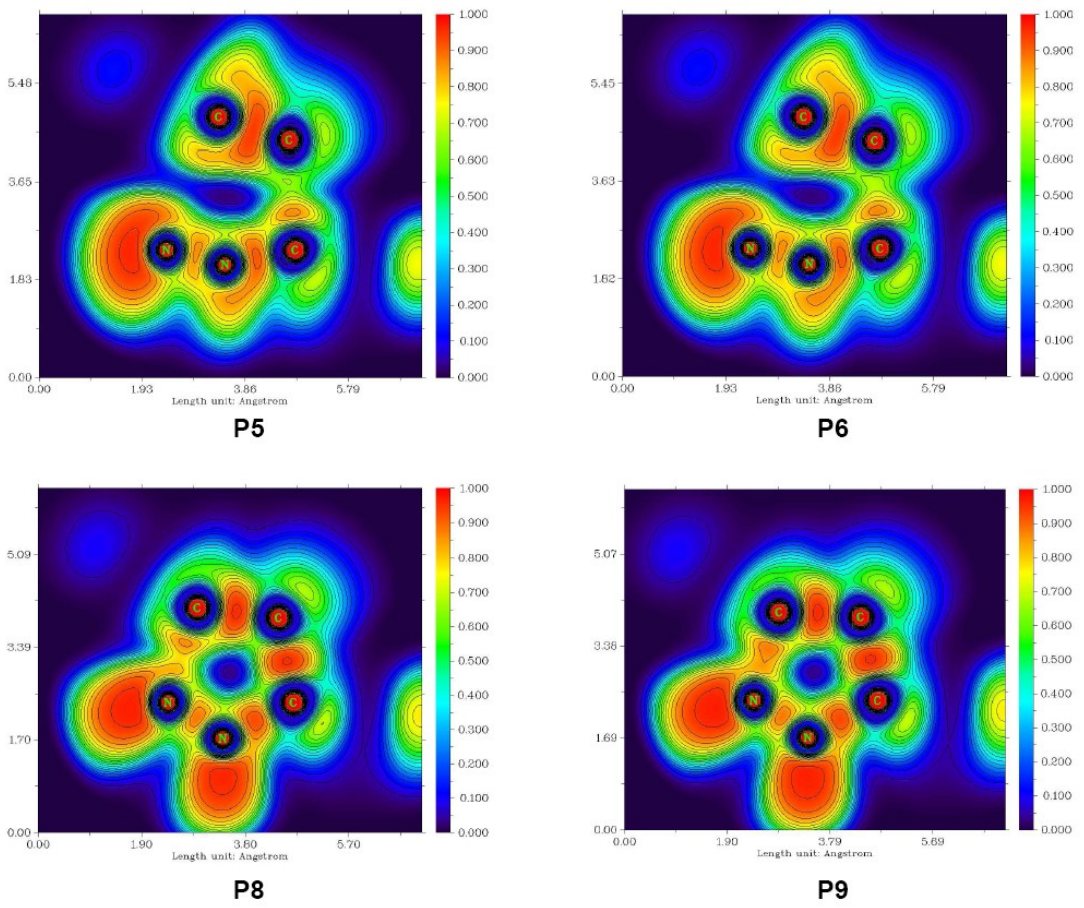

Figure S5. Colour-filled maps of the ELF for the points involved in the bond formation processes along the IRC path of the 32CA reaction between DAA **10** with DNE **11**. The ELF values (0 to 1) are mapped on a red-green-blue colour scale indicated on the right of each representation.

Table S2. B3LYP/6-31G(d,p) total energies (in a.u.), in gas phase and in benzene, of the stationary points involved in the domino reaction between DAA **10** and DNE **11**.

	Gas phase	*Benzene*
10	−487.567293	−487.571515
11	−301.401656	−301.404906
MC1	−788.971155	−788.977918
MC2	−788.971369	−788.977934
TS1	−788.956170	−788.964883
TS2	−788.944350	−788.950751
15	−789.005875	−789.011563
16	−789.000058	−789.005304
Channel I		
NO_2	−205.120386	−205.180765
NO_2H	−205.701719	−205.703624
MC3	−994.194502	−994.233152
TS3	−994.193609	−994.230972
IN1	−788.494205	−788.534755
18	−789.032689	−789.037504
MC4	−994.223062	−994.257868
TS4	−994.196417	−994.234796
MC5	−994.109349	−994.247720
12	−583.352445	−583.357356
Channel II		
TS5	−788.961544	−788.968834
N_2	−109.524129	−109.524308
13	−679.527568	−679.532700

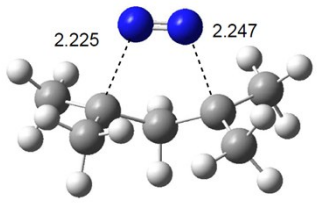

TS6

Figure S6. UB3LYP/6-31G(d,p) optimised geometry of **TS6** involved in the thermal extrusion of the nitrogen molecule from cyclic azo compound **20**.

B3LYP/6-31G(d) computed total energies, unique imaginary frequency, and cartesian coordinates of the structures involved in the domino reaction between DAA **10** and DNE **11**.

10

E(RB3LYP) = -487.567293 a.u.

C	0.30553100	-0.87490500	0.00007600
H	0.31196800	-1.95643300	-0.00045200
N	1.46739800	-0.27786100	-0.00011500
N	2.46615100	0.27314700	-0.00023500
C	-0.95312200	-0.11880200	0.00081000
O	-2.01583100	-0.72174300	-0.00038100
C	-0.87624000	1.39908500	0.00012000
H	-0.34347600	1.76759600	0.88386500
H	-0.34260600	1.76687200	-0.88340600
H	-1.89109900	1.79664500	-0.00053900

11

E(RB3LYP) = -301.401656 a.u.

C	0.00000000	1.87829100	-0.00009000
H	0.93922900	2.41701300	0.00786400
H	-0.93923400	2.41700300	-0.00806600
C	0.00000700	0.55337100	-0.00003300
N	-1.24615200	-0.23119700	0.08533900
O	-1.18693900	-1.29053300	0.69320100
O	-2.24748600	0.27889700	-0.40676100
N	1.24615200	-0.23121900	-0.08532200
O	1.18688500	-1.29071000	-0.69291800
O	2.24753600	0.27896200	0.40658100

12

E(RB3LYP) = -583.352445 a.u.

C	1.05111700	-0.02963800	0.00014800
N	0.67276700	-1.32231800	-0.00009400
N	-0.65684200	-1.29064900	-0.00009700
C	2.48496600	0.37263200	-0.00010300
O	2.76960800	1.55844000	-0.00059300
C	3.52350500	-0.72569600	0.00023600
H	3.40057600	-1.36736100	0.87884800
H	3.39976400	-1.36901000	-0.87701500
H	4.51697600	-0.27693000	-0.00057000
C	-0.06121800	0.84277800	0.00042000
H	-0.06466700	1.92012600	0.00058600
C	-1.13657000	-0.01632400	0.00032500
N	-2.55028400	0.22104800	0.00002700
O	-3.27309500	-0.78252700	-0.00042600
O	-2.92996100	1.38756100	0.00016600

H	-1.21534600	-2.13370500	-0.00003300

13

E(RB3LYP) = -679.527568 a.u.

C	-0.69171300	-0.97706200	0.35200000
H	-0.53293200	-1.98348200	-0.02254600
C	-2.02686000	-0.31387100	0.05470600
O	-2.37440600	0.66597600	0.68242200
C	-2.84950200	-0.93438500	-1.04594500
H	-2.30083500	-0.85822600	-1.99228500
H	-3.01743500	-1.99994300	-0.85304800
H	-3.80352500	-0.41427000	-1.13251100
C	0.03218000	-0.56764500	1.61504600
H	-0.46146000	0.19806700	2.20597000
H	0.62298600	-1.30995200	2.13907000
C	0.54468800	-0.11146600	0.30003500
N	1.79679800	-0.72279200	-0.22873000
O	2.56912100	0.01183900	-0.82529600
O	1.94969800	-1.91877300	-0.00204200
N	0.44316100	1.32543600	-0.11669900
O	0.01439400	1.52611300	-1.24589400
O	0.81128400	2.16182900	0.69309700

15

E(RB3LYP) = -789.005875 a.u.

C	1.45903800	-0.53240800	-0.23748100
H	1.65178200	-1.55043100	-0.59966100
N	0.99405200	-0.70081300	1.16820700
N	-0.19881800	-0.41844500	1.33162900
C	2.79781000	0.24252200	-0.25739600
O	2.89172900	1.26424000	-0.90301100
C	3.92940600	-0.35146000	0.54270800
H	3.62093900	-0.48609100	1.58451400
H	4.18347800	-1.34552400	0.15623600
H	4.80183200	0.29947400	0.48321900
C	0.30217600	0.15543900	-0.97000700
H	0.52183900	1.21258300	-1.12754300
H	0.07152700	-0.29677300	-1.93382300
C	-0.82709200	-0.00163400	0.03062500
N	-1.78327600	-1.13341100	-0.37765500
O	-2.94944100	-0.86540900	-0.59624100
O	-1.23770200	-2.22474800	-0.47930400
N	-1.68046300	1.23650600	0.27730900
O	-2.36371600	1.22351600	1.28629200
O	-1.60835600	2.12804500	-0.55899400

16

E(RB3LYP) = -789.000058 a.u.

C	-0.64774100	0.70907400	-0.59646900

H	-0.36237400	0.98299300	-1.61536700
N	-1.00471400	1.96276400	0.12350900
N	-0.19081100	2.27858600	1.00089000
C	-1.89941500	-0.21214100	-0.72596900
O	-2.17155800	-0.67412600	-1.80861400
C	-2.76230500	-0.38399100	0.50170300
H	-2.17868400	-0.57244100	1.40781700
H	-3.31274400	0.55012800	0.66616300
H	-3.46993900	-1.19628900	0.33604900
C	0.93288500	1.32369100	1.11634600
H	1.85404600	1.84846500	0.84807400
H	1.01544900	0.96707000	2.14470300
C	0.60289100	0.18046100	0.14595200
N	0.35749100	-1.16343500	0.84782800
O	0.00220000	-2.07483800	0.11646100
O	0.50237800	-1.21877600	2.06127800
N	1.79089600	-0.05543600	-0.79113000
O	2.53817300	-0.98144100	-0.52328900
O	1.93209800	0.76920200	-1.68390000

18

E(RB3LYP) = -789.032689 a.u.

C	-1.49787600	-0.07467800	0.11917700
N	-1.11708000	0.37166900	1.26888400
N	0.25678700	0.24587400	1.35199600
C	-2.92300500	-0.14445600	-0.29209500
O	-3.18119400	-0.55688100	-1.41248600
C	-3.97577700	0.29765600	0.69648800
H	-3.96221700	-0.35167500	1.57810200
H	-3.77338700	1.31323000	1.04965300
H	-4.95417500	0.25114300	0.21793100
C	-0.35335000	-0.52490700	-0.75719100
H	-0.31496200	-1.61343500	-0.86425700
H	-0.35717500	-0.09408100	-1.75941400
C	0.82456100	-0.05881100	0.08895300
N	1.56845900	1.16358200	-0.54413300
O	2.00757400	0.98424100	-1.66882300
O	1.63368700	2.18034900	0.12740000
N	1.96419100	-1.09005000	0.27143300
O	2.95451300	-0.65546800	0.84331000
O	1.77139300	-2.23267900	-0.10538600
H	0.72031800	0.93197200	1.93660500

MC1

E(RB3LYP) = -788.971155 a.u.

C	2.12713700	-1.19990700	0.20689100
H	2.20769400	-2.19896000	-0.20013900
N	1.21256900	-1.00769800	1.12024200
N	0.40319100	-0.79078700	1.89313300
C	3.05255600	-0.12808300	-0.19918600
O	3.88353900	-0.35968600	-1.06359600
C	2.91750600	1.22909600	0.46859700
H	1.93886800	1.67770800	0.26133100
H	3.01876200	1.14783300	1.55639000

H	3.69853900	1.88345600	0.08152300
C	-0.44564600	-0.16984600	-1.62235100
H	0.24389700	0.59088400	-1.96364000
H	-0.43019100	-1.15494700	-2.07124600
C	-1.32900000	0.11193100	-0.67193800
N	-2.34954200	-0.86654000	-0.25718300
O	-3.49553300	-0.45687700	-0.14871100
O	-1.96599700	-2.02526500	-0.11811900
N	-1.35540300	1.41733200	0.01631000
O	-2.02062700	1.51032500	1.03557000
O	-0.64995600	2.29759500	-0.47562100

MC2

E(RB3LYP) = -788.971369 a.u.

C	-1.66124600	0.00301900	-0.53387900
C	-1.68171300	0.88650000	-1.52293000
H	-2.20189900	1.82737500	-1.39626700
H	-1.18278700	0.66408000	-2.45721500
N	-2.24807200	0.29639700	0.78648100
O	-1.65396000	-0.14276500	1.76224400
O	-3.24456500	1.01128100	0.79545800
N	-1.04964700	-1.32863700	-0.68238000
O	-0.13909200	-1.42359200	-1.50314200
O	-1.53857500	-2.23746900	-0.02932200
C	1.75555000	0.82813800	0.87031300
H	1.35115700	0.95053700	1.86655000
N	1.36456800	1.67879700	-0.03534000
N	1.03280600	2.40492700	-0.85359300
C	2.72963800	-0.23938500	0.57004100
O	3.09124000	-0.97862600	1.47008100
C	3.22302800	-0.37572600	-0.85804200
H	2.39811000	-0.67960500	-1.51189300
H	3.62472400	0.56983700	-1.23841100
H	4.00117900	-1.13852500	-0.88451800

MC3

E(RB3LYP) = -994.194502 a.u.

C	0.86998700	0.49954300	0.06992100
H	1.55458500	-0.44456300	-0.00661700
N	0.30396300	0.53054100	1.39679700
N	-0.91839400	0.24937600	1.45050800
C	1.78961900	1.68610000	-0.18584300
O	1.66358500	2.36251600	-1.19434900
C	2.89480200	1.87409700	0.81519900
H	2.49443400	1.90498800	1.83279200
H	3.53431100	0.97936700	0.74478700
H	3.45954300	2.77987900	0.58710200
C	-0.31302400	0.34108600	-0.89353800
H	-0.53384600	1.28186500	-1.40084500
H	-0.15026000	-0.44021000	-1.63610300
C	-1.42650700	-0.00703200	0.07044600
N	-1.88960900	-1.46646000	-0.06331000
O	-2.45095300	-1.73852600	-1.12037600

O	-1.64217500	-2.23463700	0.84775900
N	-2.71370100	0.80779900	-0.06115800
O	-3.69392100	0.36064500	0.52278100
O	-2.65880100	1.87494000	-0.66027000
N	3.42192100	-2.04242600	-0.36991000
O	2.16542200	-1.90603800	-0.53639600
O	4.03218000	-1.09088600	0.15976400

MC4

E(RB3LYP) = -994.223062 a.u.

C	-0.57442100	1.06577400	0.05400100
H	-2.10394800	-1.12438000	-0.59628500
N	-0.76222200	-0.21670300	-0.22472300
N	0.33952100	-0.96416900	-0.22422000
C	-1.60820900	2.07210500	0.08360300
O	-1.33781600	3.25097000	0.34765500
C	-3.04206800	1.64896500	-0.21108100
H	-3.11942500	1.15016700	-1.18223700
H	-3.39728400	0.93624700	0.54022100
H	-3.67307700	2.53978900	-0.20209000
C	0.88108700	1.30401400	0.35952900
H	1.34505500	2.09558600	-0.23231000
H	1.05600400	1.52959900	1.41583100
C	1.42595000	-0.08966700	0.04472600
N	2.28794900	-0.70732800	1.16166300
O	2.97630900	-1.67195600	0.84507600
O	2.15726400	-0.27026600	2.30249100
N	2.45609300	-0.01766300	-1.15797200
O	2.13788200	-0.51372400	-2.22331300
O	3.48453100	0.61937900	-0.93511600
O	-3.62611900	-1.60970600	0.97737000
O	-2.83949700	-1.71972100	-1.02620100
N	-3.78159600	-2.06756300	-0.13067600

MC5

E(RB3LYP) = -994.109349 a.u.

C	0.65109300	-1.26040000	0.16558400
N	-0.27602600	-2.15429400	0.26041600
N	-1.48991400	-1.51069900	0.39240200
C	2.09010100	-1.60942700	0.06749100
O	2.90573400	-0.70597800	-0.04550600
C	2.47543800	-3.06897800	0.11280800
H	2.19992300	-3.50181300	1.08004900
H	1.93563300	-3.63572300	-0.65158800
H	3.55127700	-3.15705300	-0.03940300
C	0.12116000	0.15389200	0.17390900
H	0.35661100	0.68109800	1.10369000
H	0.47738200	0.77268300	-0.65145100
C	-1.37490500	-0.12567400	0.11166200
N	-1.99821000	0.25829500	-1.27086300
O	-1.86629100	1.42661100	-1.59820000
O	-2.54393400	-0.63438400	-1.89907300
N	-2.24634300	0.67590900	1.10849600

O	-3.45188200	0.53040600	0.95794700
O	-1.68343200	1.32348500	1.97343000
H	-2.29141100	-2.01430800	0.03036800
N	3.13876500	2.28683300	-0.16742800
O	2.79325100	2.14770700	0.97474500
O	2.60847200	2.09044600	-1.22853700

IN1

E(RB3LYP) = -788.494205 a.u.

C	1.49723500	0.05556800	-0.06008900
N	1.05963100	-0.04977600	-1.31240500
N	-0.26125200	-0.03651500	-1.42945100
C	2.88014200	0.02962900	0.31935200
O	3.24262000	0.12319100	1.50350600
C	3.92227800	-0.11784900	-0.78783500
H	3.46631900	-0.21424800	-1.77418800
H	4.58499000	0.75536300	-0.76993600
H	4.54361100	-0.99545600	-0.57561300
C	0.33468000	0.21521000	0.88931300
H	0.31084900	-0.51293300	1.70296100
H	0.27944700	1.21381500	1.33197000
C	-0.80733400	0.04170200	-0.11122100
N	-1.85466300	1.16171000	-0.09153300
O	-2.92389900	0.91979600	-0.64654600
O	-1.52890000	2.25654100	0.36635500
N	-1.67662900	-1.22894000	0.25967100
O	-1.63447400	-2.19794700	-0.47728600
O	-2.28245100	-1.16626200	1.32943600

TS1

E(RB3LYP) = -788.956170 a.u.
1 imaginary frequency: -378.5317 cm^{-1}

C	1.50691000	-1.01821800	0.14243600
H	1.59637300	-2.08635000	-0.03805900
N	0.85955800	-0.75093500	1.30182000
N	-0.01135500	-0.34917300	1.90973900
C	2.75583900	-0.21205100	-0.17718900
O	3.45573900	-0.62513000	-1.07708300
C	2.98572300	1.07703800	0.56917200
H	2.10709600	1.72499900	0.47190700
H	3.14456200	0.88234900	1.63609600
H	3.86394000	1.57319100	0.15652600
C	0.08092800	-0.41499400	-1.16296400
C	-1.05462700	0.03995100	-0.49807700
H	0.66789200	0.33771400	-1.67412400
H	-0.00461900	-1.38278200	-1.64104900
N	-2.09881400	-0.91721100	-0.18572000
O	-3.26135400	-0.56387500	-0.05254200
O	-1.69709200	-2.09141900	-0.08560900
N	-1.21385500	1.45276900	-0.23159200
O	-2.28997200	1.90666200	0.13048200
O	-0.17889900	2.13280900	-0.37916100

TS2

E(RB3LYP) = -788.944350 a.u.
1 imaginary frequency: -430.1989 cm^{-1}

C	-0.86001500	0.76810300	-0.88764600
H	-0.36064400	0.87823100	-1.84740400
N	-0.87720600	1.87691100	-0.14815300
N	-0.33150300	2.41612900	0.73507100
C	-2.01037600	-0.20719800	-0.84020500
O	-2.08377000	-1.02421000	-1.73538400
C	-2.95337100	-0.15059900	0.33701000
H	-2.41636800	-0.42166400	1.25383300
H	-3.35902200	0.85756400	0.47149400
H	-3.76453400	-0.85970800	0.17260100
C	1.08420800	1.19767600	1.26203600
C	0.97112000	0.07050000	0.44418200
H	1.88537400	1.89362600	1.04146000
H	0.78942700	1.08978700	2.29801800
N	0.36242700	-1.15390400	0.97781200
O	0.34617800	-2.16098700	0.28619000
O	-0.17548600	-1.04347800	2.08813300
N	1.94981300	-0.06382700	-0.64650000
O	2.56171300	-1.11068000	-0.78133000
O	2.11532000	0.95986800	-1.32134300

TS3

E(RB3LYP) = -994.193609 a.u.
1 imaginary frequency: -569.9348 cm^{-1}

C	-0.88652800	-0.56009300	0.04018300
H	-1.53802400	0.54789500	-0.10782200
N	-0.37364000	-0.54694400	1.35696900
N	0.85345300	-0.24875900	1.44785000
C	-1.90348700	-1.62088100	-0.24083700
O	-1.92229600	-2.19276900	-1.32440200
C	-2.94733400	-1.85893200	0.82476500
H	-2.48496700	-1.99600800	1.80588400
H	-3.56693100	-0.95402600	0.87757000
H	-3.55785300	-2.72247600	0.55351500
C	0.31824500	-0.45861700	-0.90300400
H	0.56308600	-1.42717900	-1.34326900
H	0.18902100	0.27021900	-1.70372700
C	1.39516700	-0.04541900	0.08026400
N	1.83841600	1.41793400	-0.12067100
O	2.40671400	1.64844100	-1.18504500
O	1.57206600	2.22697000	0.74814000
N	2.70263800	-0.83621700	0.01509000
O	3.66453500	-0.33837100	0.58879700
O	2.68159400	-1.93720300	-0.52334500
N	-3.13286700	2.14087200	-0.29196000
O	-1.89782800	1.81841400	-0.51363300
O	-3.83937400	1.28164600	0.24182200

TS4

E(RB3LYP) = -994.196417 a.u.
1 imaginary frequency: -1005.5865 cm^{-1}

C	-1.03315700	-0.94550500	0.14170700
N	-0.60270700	-1.21098000	1.34476600
N	0.75651600	-0.87992500	1.33600300
C	-2.42737200	-1.27623300	-0.24835000
O	-2.75497600	-1.28839700	-1.42611000
C	-3.41280900	-1.56766700	0.86507100
H	-2.94668900	-2.13250500	1.67509400
H	-3.73886100	-0.60549700	1.27575400
H	-4.27720800	-2.09633500	0.45772600
C	-0.07933200	-0.22810100	-0.70025300
H	0.01995400	-0.47149700	-1.75306500
H	-0.59361300	1.09661000	-0.75684300
C	1.14044300	-0.27230300	0.12607400
N	1.84768300	1.12413400	0.36425700
O	2.35816700	1.64893600	-0.61422100
O	1.78991200	1.60001300	1.49339400
N	2.40162400	-1.06867900	-0.48460500
O	3.41585500	-1.06943200	0.21055100
O	2.24836100	-1.69542700	-1.52144000
H	1.13308700	-0.51810500	2.20162000
N	-2.00537100	2.65791400	-0.32427800
O	-0.90119100	2.28593700	-0.92732700
O	-2.59457000	1.78199000	0.30280600

TS5

E(UB3LYP) = -788.961544 a.u.
1 imaginary frequency: -411.5592 cm^{-1}

C	1.47988800	-0.33474400	-0.28936100
C	-1.04034200	0.08817800	-0.19672800
H	1.43868600	-1.40430300	-0.46511100
N	0.99749600	-0.59146900	1.68620200
N	-0.10551500	-0.47448300	1.89197500
C	2.82832000	0.33052500	-0.27517300
O	2.91547800	1.51358000	-0.56442400
C	4.00397600	-0.52803100	0.10968300
H	3.82248000	-1.01717000	1.07285300
H	4.14569900	-1.32216900	-0.63251300
H	4.90325700	0.08506700	0.16695600
C	0.30200000	0.47260900	-0.66660900
H	0.47491600	1.53261700	-0.48331900
H	0.32874700	0.33826600	-1.77121200
N	-1.56611100	-1.20608900	-0.52477900
O	-2.77088100	-1.43442800	-0.47534800
O	-0.70687900	-2.04751100	-0.86034800
N	-1.98913300	1.14626900	0.07921500
O	-2.95268100	0.89105800	0.79542600
O	-1.72428500	2.26441000	-0.38365700